Phase effects in laser-induced electron-positron pair creation

K. Krajewska* and J. Z. Kamiński
Institute of Theoretical Physics, Faculty of Physics, University of Warsaw, Hoża 69, 00-681 Warsaw, Poland
(Received 2 February 2012; published 9 April 2012)

Probability rates of electron-positron pair creation in collisions of a relativistic nucleus with a two-color laser field are calculated using the S-matrix approach. The case when both components of the laser field have commensurate frequencies and comparable strengths is considered. Pronounced interference effects are observed in angular distributions of created particles as well as in the total probability rates of pair production. These interference effects show a significant phase dependence of the pair-creation process.

DOI: 10.1103/PhysRevA.85.043404 PACS number(s): 34.50.Rk, 32.80.Wr, 12.20.Ds

I. INTRODUCTION

Recent technological progress leading to development of ultrashort laser pulses with well-defined temporal characteristics makes it possible to study and to effectively control laser-induced processes. Strategies for controlling photoprocesses utilize different properties of laser radiation. One of them is the so-called coherent phase control which originally was suggested as means to manipulate molecular reactions (for a review, see [1]). It appeared that by applying a bichromatic laser field such that the phase difference of both color fields is varied, the efficiency of photoprocesses could be actively manipulated (for a review, see [2]). The same can be achieved by changing the carrier-envelope phase of a single laser pulse or, similarly, of a laser pulse train. With such techniques it becomes possible, for instance, to control the photoionization probability yields, the electron dynamics in strong magnetic fields, the fragmentation and space orientation of molecules, and the efficiency of high-harmonic generation. The purpose of the present paper is to investigate how the properties of another laser-induced process, the so-called nonlinear Bethe-Heitler electron-positron pair-creation process, depend on a phase coherence of a driving laser field. Here, in particular, the emphasis will be put on similarities and differences with strong-field ionization.

The nonlinear Bethe-Heitler process, in which electron-positron pairs are created in collisions of a superintense laser beam with a beam of relativistic targets, has been considered by many authors for a monochromatic plane-wave laser field (for a review, see, for instance, Ref. [3], and also Refs. [4–26]). We find interesting to generalize these investigations by introducing a second component of the laser field. More precisely, we shall consider two plane-wave fields of commensurate frequencies which propagate in the same direction but, in general, that are shifted in phase. A similar situation has been considered for the pair-creation process by a nonlaser photon, in which case strong interference effects were observed [27–30]. It is the purpose of the present paper to investigate similar effects and their dependence on the relative phase between both component fields for the nonlinear Bethe-Heitler process. In addition, we shall model a laser pulse train as a bichromatic laser field, in which case the carrier-envelope phase effects in the pair-creation process can also be studied.

This paper is organized as follows. In Sec. II, we present the theory of the nonlinear Bethe-Heitler process by a two-mode laser field, which accounts for nuclear recoil of target particles. In Sec. III, the angular distributions of created particles are studied as a function of the relative phase between both color fields. In Sec. IV, we discuss possibility of applying the presented theory to account for a train of laser pulses. For the chosen four-vector potential describing such a laser pulse train, three different representations are investigated. The results for the total probability rates of pair production for different representations of the laser pulse train are presented in Sec. V. Finally, we summarize our results and discuss our conclusions in Sec. VI.

II. THEORY

In the following, we keep the notation and mathematical convention introduced in our recent works on the multiphoton electron-positron pair creation [21,25,26]. In particular, we present formulas in which we put $\hbar = 1$; however our numerical results are presented either in relativistic units such that $c = m_e = 1$, where m_e is the electron mass, or in arbitrary units. By convention, we write $a \cdot b = a^\mu b_\mu$ ($\mu = 0,1,2,3$) for a product of any two four-vectors a and b, and $\not{a} = \gamma \cdot a = \gamma^\mu a_\mu$ where γ^μ are the Dirac gamma matrices; here and in what follows, the Einstein summation convention is used.

We consider a two-color laser field represented by the four-vector potential,

$$A^\mu(k \cdot x) = \sum_{i=1}^{2} A_i^\mu(k \cdot x), \tag{1}$$

such that each component A_i^μ describes an elliptically polarized plane wave field,

$$A_i^\mu(k \cdot x) = A_{i0}\big[\varepsilon_{i1}^\mu \cos\delta_i \cos(n_i k \cdot x + \chi_i) + \varepsilon_{i2}^\mu \sin\delta_i \sin(n_i k \cdot x + \chi_i)\big]. \tag{2}$$

Here, A_{i0} denotes the strength of the ith vector potential, while the polarization four-vectors are $\varepsilon_{ij} = (0, \boldsymbol{\varepsilon}_{ij})$ ($j = 1,2$), such that, for each wave, $\varepsilon_{i1}^2 = \varepsilon_{i2}^2 = -\boldsymbol{\varepsilon}_{i1}^2 = -\boldsymbol{\varepsilon}_{i2}^2 = -1$ and $\varepsilon_{i1} \cdot \varepsilon_{i2} = -\boldsymbol{\varepsilon}_{i1} \cdot \boldsymbol{\varepsilon}_{i2} = 0$. In addition, δ_i is an angle describing the ellipticity of the ith field and χ_i describes its phase. $k = (\omega/c)(1, \boldsymbol{n})$ is the wave four-vector, with ω being the angular

*katarzyna.krajewska@fuw.edu.pl

frequency of the laser-field oscillations and $\boldsymbol{n}$ being the laser field propagation direction. Since, for the vector potential given by Eqs. (1) and (2), it holds that $k \cdot A_1 = 0 = k \cdot A_2$ and also $k^2 = 0$, one can derive exact relativistic solutions of the Dirac equation coupled to the electromagnetic field.

A. Volkov waves

For a spin $\frac{1}{2}$ particle of mass m and charge $\mathcal{Z}e$ (where $\mathcal{Z}$ is related to the atomic number Z such that $|\mathcal{Z}| = Z$, and where $e < 0$ is the electron charge) that is embedded in the electromagnetic field, the Dirac equation has the form

$$(i\partial\!\!\!/ - \mathcal{Z}eA\!\!\!/ - mc)\psi^{(\beta)}_{p,\lambda}(x) = 0, \tag{3}$$

where the solutions $\psi^{(\beta)}_{p,\lambda}(x)$ are the so-called Volkov waves [31]. In our case, the Volkov solutions are labeled by three indices; while p and λ refer to the particle momentum outside the laser focus and to its spin projection, respectively, β distinguishes between positive- and negative-energy states that correspond to a particle ($\beta = +1$) or to an antiparticle ($\beta = -1$). In the most general form, these solutions are given by (see, Ref. [21])

$$\psi^{(\beta)}_{p,\lambda}(x) = \sqrt{\frac{mc^2}{VE_{\boldsymbol{p}}}}\left(1 - \frac{\beta\mathcal{Z}e}{2k\cdot p}A\!\!\!/k\!\!\!/\right) u^{(\beta)}_{p,\lambda} e^{-i\beta S^{(\beta)}_p(x)}, \tag{4}$$

where $u^{(\beta)}_{p,\lambda}$ are four-spinors satisfying the field-free equation, $(p\!\!\!/ - \beta mc)u^{(\beta)}_{p,\lambda} = 0$, while the phase factor is

$$S^{(\beta)}_p(x) = p\cdot x + \int^{k\cdot x}\left[\beta\mathcal{Z}e\frac{A(\phi)\cdot p}{k\cdot p} - (\mathcal{Z}e)^2\frac{A^2(\phi)}{2k\cdot p}\right]d\phi. \tag{5}$$

In the present case, when the four-vector potential is represented by a superposition of monochromatic waves [see, Eqs. (1) and (2)], the phase (5) can be rewritten as

$$S^{(\beta)}_p(x) = \bar{p}\cdot x + Q^{(\beta)}_p(k\cdot x), \tag{6}$$

where the so-called dressed four-momentum of a particle in a bichromatic laser field has been introduced,

$$\bar{p} = p + \sum_{i=1}^{2}\frac{(\mathcal{Z}eA_{i0})^2}{4k\cdot p}k. \tag{7}$$

Moreover, the laser-dressed four-momentum $\bar{p}$ satisfies the effective-mass on-shell relation $\bar{p}^2 = (\bar{m}c)^2$, where the effective mass $\bar{m}$ equals

$$\bar{m}^2 = m^2 + \frac{1}{2}m_e^2\mathcal{Z}^2\sum_{i=1}^{2}\mu_i^2, \tag{8}$$

with μ_i defining the normalized amplitude of each color field,

$$\mu_i = \frac{|eA_{i0}|}{m_e c}, \quad i = 1,2. \tag{9}$$

At this point, let us also introduce the normalized amplitude of the two-color field,

$$\mu = \sqrt{\sum_{i=1}^{2}\mu_i^2}, \tag{10}$$

with μ_i defined above. In Eq. (6), we have also introduced the function $Q^{(\beta)}_p(k\cdot x)$ which, for our choice of the four-vector potential, equals

$$\begin{aligned}
Q^{(\beta)}_p(k\cdot x) &= \beta\sum_{i=1}^{2}\frac{\mathcal{Z}eA_{i0}}{n_i}\frac{\varepsilon_{i1}\cdot p}{k\cdot p}\cos\delta_i\sin(n_i k\cdot x + \chi_i)\\
&\quad -\beta\sum_{i=1}^{2}\frac{\mathcal{Z}eA_{i0}}{n_i}\frac{\varepsilon_{i2}\cdot p}{k\cdot p}\sin\delta_i\cos(n_i k\cdot x + \chi_i)\\
&\quad +\sum_{i=1}^{2}\frac{(\mathcal{Z}eA_{i0})^2}{8n_i}\frac{1}{k\cdot p}\cos(2\delta_i)\sin[2(n_i k\cdot x + \chi_i)]\\
&\quad +\frac{(\mathcal{Z}e)^2A_{10}A_{20}}{2(n_1+n_2)}\frac{1}{k\cdot p}\sin[(n_1+n_2)k\cdot x + \chi_1 + \chi_2]\\
&\quad \times(\boldsymbol{\varepsilon}_{11}\cdot\boldsymbol{\varepsilon}_{21}\cos\delta_1\cos\delta_2 - \boldsymbol{\varepsilon}_{12}\cdot\boldsymbol{\varepsilon}_{22}\sin\delta_1\sin\delta_2)\\
&\quad -\frac{(\mathcal{Z}e)^2A_{10}A_{20}}{2(n_1+n_2)}\frac{1}{k\cdot p}\cos[(n_1+n_2)k\cdot x + \chi_1 + \chi_2]\\
&\quad \times(\boldsymbol{\varepsilon}_{11}\cdot\boldsymbol{\varepsilon}_{22}\cos\delta_1\sin\delta_2 + \boldsymbol{\varepsilon}_{12}\cdot\boldsymbol{\varepsilon}_{21}\sin\delta_1\cos\delta_2)\\
&\quad +\frac{(\mathcal{Z}e)^2A_{10}A_{20}}{2(n_1-n_2)}\frac{1}{k\cdot p}\sin[(n_1-n_2)k\cdot x + \chi_1 - \chi_2]\\
&\quad \times(\boldsymbol{\varepsilon}_{11}\cdot\boldsymbol{\varepsilon}_{21}\cos\delta_1\cos\delta_2 + \boldsymbol{\varepsilon}_{12}\cdot\boldsymbol{\varepsilon}_{22}\sin\delta_1\sin\delta_2)\\
&\quad +\frac{(\mathcal{Z}e)^2A_{10}A_{20}}{2(n_1-n_2)}\frac{1}{k\cdot p}\cos[(n_1-n_2)k\cdot x + \chi_1 - \chi_2]\\
&\quad \times(\boldsymbol{\varepsilon}_{11}\cdot\boldsymbol{\varepsilon}_{22}\cos\delta_1\sin\delta_2 - \boldsymbol{\varepsilon}_{12}\cdot\boldsymbol{\varepsilon}_{21}\sin\delta_1\cos\delta_2).
\end{aligned} \tag{11}$$

Thus, the Volkov waves (4) can be written in the form

$$\begin{aligned}
\psi^{(\beta)}_{p,\lambda}(x) &= \sqrt{\frac{mc^2}{VE_{\boldsymbol{p}}}}\left(1 - \frac{\beta\mathcal{Z}e}{2k\cdot p}A\!\!\!/k\!\!\!/\right)u^{(\beta)}_{p,\lambda}\\
&\quad\times\exp\left\{-i\beta\left[\bar{p}\cdot x + Q^{(\beta)}_p(k\cdot x)\right]\right\},
\end{aligned} \tag{12}$$

with the aforementioned definitions of $\bar{p}$ and $Q^{(\beta)}_p(k\cdot x)$.

B. Four-currents

With the above Volkov solutions for the ingoing particle (antiparticle) of four-momentum p_i and spin projection λ_i and the outgoing particle (antiparticle) of four-momentum p_f and spin projection λ_f, the four-current

$$j^{\mu}_{p_\mathrm{f}p_\mathrm{i}}(x) = \bar{\psi}^{(\beta_\mathrm{f})}_{p_\mathrm{f},\lambda_\mathrm{f}}(x)\gamma^{\mu}\psi^{(\beta_\mathrm{i})}_{p_\mathrm{i},\lambda_\mathrm{i}}(x) \tag{13}$$

can be evaluated explicitly. Here, β_i and β_f denote either a particle or an antiparticle in the initial and final states, respectively. Substituting the corresponding Volkov waves (12) into Eq. (13), we obtain

$$\begin{aligned}
j^{\mu}_{p_\mathrm{f}p_\mathrm{i}}(x) &= \frac{mc^2}{V\sqrt{E_{\boldsymbol{p}_\mathrm{f}}E_{\boldsymbol{p}_\mathrm{i}}}}\bar{u}^{(\beta_\mathrm{f})}_{p_\mathrm{f}\lambda_\mathrm{f}}\left(1 + \beta_\mathrm{f}\frac{\mathcal{Z}eA\!\!\!/k\!\!\!/}{2k\cdot p_\mathrm{f}}\right)\\
&\quad\times\gamma^{\mu}\left(1 - \beta_\mathrm{i}\frac{\mathcal{Z}eA\!\!\!/k\!\!\!/}{2k\cdot p_\mathrm{i}}\right)u^{(\beta_\mathrm{i})}_{p_\mathrm{i}\lambda_\mathrm{i}}\exp\left[i(\beta_\mathrm{f}\bar{p}_\mathrm{f} - \beta_\mathrm{i}\bar{p}_\mathrm{i})\cdot x\right]\\
&\quad\times\exp\left\{i\left[\beta_\mathrm{f}Q^{(\beta_\mathrm{f})}_{p_\mathrm{f}}(k\cdot x) - \beta_\mathrm{i}Q^{(\beta_\mathrm{i})}_{p_\mathrm{i}}(k\cdot x)\right]\right\},
\end{aligned} \tag{14}$$

where the last line in this equation is a periodic function of $k\cdot x$ and thus can be Fourier-decomposed with respect to $k\cdot x$.

Before we do this, let us introduce coefficients,

$$\frac{\mathcal{Z}eA_{i0}}{n_i}\left(\frac{\varepsilon_{i1}\cdot p_{\rm i}}{k\cdot p_{\rm i}}-\frac{\varepsilon_{i1}\cdot p_{\rm f}}{k\cdot p_{\rm f}}\right)\cos\delta_i = a_i\cos\eta_i, \tag{15}$$

$$-\frac{\mathcal{Z}eA_{i0}}{n_i}\left(\frac{\varepsilon_{i2}\cdot p_{\rm i}}{k\cdot p_{\rm i}}-\frac{\varepsilon_{i2}\cdot p_{\rm f}}{k\cdot p_{\rm f}}\right)\sin\delta_i = a_i\sin\eta_i, \tag{16}$$

$$\frac{(\mathcal{Z}eA_{i0})^2}{8n_i}\left(\frac{\beta_{\rm i}}{k\cdot p_{\rm i}}-\frac{\beta_{\rm f}}{k\cdot p_{\rm f}}\right)\cos(2\delta_i) = b_i, \tag{17}$$

for $i = 1,2$ and also

$$\frac{(\mathcal{Z}e)^2A_{10}A_{20}}{2(n_1+n_2)}\left(\frac{\beta_{\rm i}}{k\cdot p_{\rm i}}-\frac{\beta_{\rm f}}{k\cdot p_{\rm f}}\right)(\boldsymbol{\varepsilon}_{11}\cdot\boldsymbol{\varepsilon}_{21}\cos\delta_1\cos\delta_2-\boldsymbol{\varepsilon}_{12}\cdot\boldsymbol{\varepsilon}_{22}\sin\delta_1\sin\delta_2) = c_{12}\cos\xi_{12}, \tag{18}$$

$$-\frac{(\mathcal{Z}e)^2A_{10}A_{20}}{2(n_1+n_2)}\left(\frac{\beta_{\rm i}}{k\cdot p_{\rm i}}-\frac{\beta_{\rm f}}{k\cdot p_{\rm f}}\right)(\boldsymbol{\varepsilon}_{11}\cdot\boldsymbol{\varepsilon}_{22}\cos\delta_1\sin\delta_2+\boldsymbol{\varepsilon}_{12}\cdot\boldsymbol{\varepsilon}_{21}\sin\delta_1\cos\delta_2) = c_{12}\sin\xi_{12}, \tag{19}$$

$$\frac{(\mathcal{Z}e)^2A_{10}A_{20}}{2(n_1-n_2)}\left(\frac{\beta_{\rm i}}{k\cdot p_{\rm i}}-\frac{\beta_{\rm f}}{k\cdot p_{\rm f}}\right)(\boldsymbol{\varepsilon}_{11}\cdot\boldsymbol{\varepsilon}_{21}\cos\delta_1\cos\delta_2+\boldsymbol{\varepsilon}_{12}\cdot\boldsymbol{\varepsilon}_{22}\sin\delta_1\sin\delta_2) = d_{12}\cos\zeta_{12}, \tag{20}$$

$$\frac{(\mathcal{Z}e)^2A_{10}A_{20}}{2(n_1-n_2)}\left(\frac{\beta_{\rm i}}{k\cdot p_{\rm i}}-\frac{\beta_{\rm f}}{k\cdot p_{\rm f}}\right)(\boldsymbol{\varepsilon}_{11}\cdot\boldsymbol{\varepsilon}_{22}\cos\delta_1\sin\delta_2-\boldsymbol{\varepsilon}_{12}\cdot\boldsymbol{\varepsilon}_{21}\sin\delta_1\cos\delta_2) = d_{12}\sin\zeta_{12}, \tag{21}$$

with the help of which we can explicitly write

$$\begin{aligned}\exp\left\{i\left[\beta_{\rm f}Q_{p_{\rm f}}^{(\beta_{\rm f})}(k\cdot x)-\beta_{\rm i}Q_{p_{\rm i}}^{(\beta_{\rm i})}(k\cdot x)\right]\right\} = \prod_{i=1}^{2}\exp\{&-ia_i\sin(n_ik\cdot x+\chi_i+\eta_i)-ib_i\sin[2(n_ik\cdot x+\chi_i)]\}\\ &\times\exp\{-ic_{12}\sin[(n_1+n_2)k\cdot x+\chi_1+\chi_2+\xi_{12}]\\ &-id_{12}\sin[(n_1-n_2)k\cdot x+\chi_1-\chi_2+\zeta_{12}]\}.\end{aligned} \tag{22}$$

Using the following Fourier expansions:

$$e^{-iu\sin\theta} = \sum_{N=-\infty}^{\infty}J_N(u)e^{-iN\theta}, \tag{23}$$

$$e^{-iu\sin\theta-iv\sin(2\theta+\eta)} = \sum_{N=-\infty}^{\infty}B_N(u,v,\eta)e^{-iN\theta}, \tag{24}$$

where $J_N(u)$ are the ordinary and $B_N(u,v,\theta)$ are the generalized Bessel functions, we derive the Fourier decomposition of $\exp\{i[\beta_{\rm f}Q_{p_{\rm f}}^{(\beta_{\rm f})}(k\cdot x)-\beta_{\rm i}Q_{p_{\rm i}}^{(\beta_{\rm i})}(k\cdot x)]\}$,

$$\exp\left\{i\left[\beta_{\rm f}Q_{p_{\rm f}}^{(\beta_{\rm f})}(k\cdot x)-\beta_{\rm i}Q_{p_{\rm i}}^{(\beta_{\rm i})}(k\cdot x)\right]\right\} = \sum_N e^{-iNk\cdot x}G_N, \tag{25}$$

where the coefficients G_N are

$$\begin{aligned}G_N = \sum_{K=-\infty}^{\infty}\sum_{K'=-\infty}^{\infty}\sum_{M=-\infty}^{\infty}\sum_{M'=-\infty}^{\infty}&B_K(a_1,b_1,-2\eta_1)B_{K'}(a_2,b_2,-2\eta_2)J_M(c_{12})J_{M'}(d_{12})e^{-iK(\chi_1+\eta_1)}\\ &\times\exp[-iK'(\chi_2+\eta_2)-iM(\chi_1+\chi_2+\xi_{12})-iM'(\chi_1-\chi_2+\zeta_{12})]\delta_{N,\,Kn_1+K'n_2+M(n_1+n_2)+M'(n_1-n_2)}.\end{aligned} \tag{26}$$

Applying the Fourier expansion (25) into the definition of the four-current (14), we find that

$$j^{\mu}_{p_{\rm f}p_{\rm i}}(x) = \frac{mc^2}{V\sqrt{E_{\boldsymbol{p}_{\rm f}}E_{\boldsymbol{p}_{\rm i}}}}\sum_{N=-\infty}^{\infty}\exp\left[-i(Nk+\beta_{\rm i}\bar{p}_{\rm i}-\beta_{\rm f}\bar{p}_{\rm f})\cdot x\right]\mathcal{J}^{\mu}_N(p_{\rm f},\lambda_{\rm f},\beta_{\rm f};p_{\rm i},\lambda_{\rm i},\beta_{\rm i}), \tag{27}$$

where the coefficients $\mathcal{J}^{\mu}_{N}(p_{\rm f},\lambda_{\rm f},\beta_{\rm f};p_{\rm i},\lambda_{\rm i},\beta_{\rm i})$ are given by

$$\begin{aligned}
\mathcal{J}^{\mu}_{N}(p_{\rm f},\lambda_{\rm f},\beta_{\rm f};p_{\rm i},\lambda_{\rm i},\beta_{\rm i}) = \bar{u}^{(\beta_{\rm f})}_{p_{\rm f},\lambda_{\rm f}}\Bigg[&\gamma^{\mu}G_N + \sum_{i=1}^{2}\frac{\mathcal{Z}eA_{i0}}{4}\cos\delta_i\left(\frac{\beta_{\rm f}}{k\cdot p_{\rm f}}\not{\epsilon}_{i1}\not{k}\gamma^{\mu} - \frac{\beta_{\rm i}}{k\cdot p_{\rm i}}\gamma^{\mu}\not{\epsilon}_{i1}\not{k}\right)\left(e^{i\chi_i}G_{N+n_i} + e^{-i\chi_i}G_{N-n_i}\right)\\
&+\sum_{i=1}^{2}\frac{\mathcal{Z}eA_{i0}}{4i}\sin\delta_i\left(\frac{\beta_{\rm f}}{k\cdot p_{\rm f}}\not{\epsilon}_{i2}\not{k}\gamma^{\mu} - \frac{\beta_{\rm i}}{k\cdot p_{\rm i}}\gamma^{\mu}\not{\epsilon}_{i2}\not{k}\right)\left(e^{i\chi_i}G_{N+n_i} - e^{-i\chi_i}G_{N-n_i}\right)\\
&-\sum_{i=1}^{2}\frac{\beta_{\rm i}\beta_{\rm f}(\mathcal{Z}eA_{i0})^2}{16(k\cdot p_{\rm i})(k\cdot p_{\rm f})}\cos^2\delta_i\not{\epsilon}_{i1}\not{k}\gamma^{\mu}\not{\epsilon}_{i1}\not{k}\left(e^{2i\chi_i}G_{N+2n_i} + 2G_N + e^{-2i\chi_i}G_{N-2n_i}\right)\\
&+\sum_{i=1}^{2}\frac{\beta_{\rm i}\beta_{\rm f}(\mathcal{Z}eA_{i0})^2}{16(k\cdot p_{\rm i})(k\cdot p_{\rm f})}\sin^2\delta_i\not{\epsilon}_{i2}\not{k}\gamma^{\mu}\not{\epsilon}_{i2}\not{k}\left(e^{2i\chi_i}G_{N+2n_i} - 2G_N + e^{-2i\chi_i}G_{N-2n_i}\right)\\
&-\sum_{i=1}^{2}\frac{\beta_{\rm i}\beta_{\rm f}(\mathcal{Z}eA_{i0})^2}{32i(k\cdot p_{\rm i})(k\cdot p_{\rm f})}\sin 2\delta_i(\not{\epsilon}_{i1}\not{k}\gamma^{\mu}\not{\epsilon}_{i2}\not{k} + \not{\epsilon}_{i2}\not{k}\gamma^{\mu}\not{\epsilon}_{i1}\not{k})\\
&\times\left(e^{2i\chi_i}G_{N+2n_i} - e^{-2i\chi_i}G_{N-2n_i}\right)\\
&-\frac{\beta_{\rm i}\beta_{\rm f}(\mathcal{Z}e)^2A_{10}A_{20}}{16(k\cdot p_{\rm i})(k\cdot p_{\rm f})}\cos\delta_1\cos\delta_2(\not{\epsilon}_{11}\not{k}\gamma^{\mu}\not{\epsilon}_{21}\not{k} + \not{\epsilon}_{21}\not{k}\gamma^{\mu}\not{\epsilon}_{11}\not{k})\\
&\times\left(e^{i(\chi_1+\chi_2)}G_{N+n_1+n_2} + e^{i(\chi_1-\chi_2)}G_{N+n_1-n_2} + e^{-i(\chi_1-\chi_2)}G_{N-n_1+n_2} + e^{-i(\chi_1+\chi_2)}G_{N-n_1-n_2}\right)\\
&-\frac{\beta_{\rm i}\beta_{\rm f}(\mathcal{Z}e)^2A_{10}A_{20}}{16i(k\cdot p_{\rm i})(k\cdot p_{\rm f})}\cos\delta_1\sin\delta_2(\not{\epsilon}_{11}\not{k}\gamma^{\mu}\not{\epsilon}_{22}\not{k} + \not{\epsilon}_{22}\not{k}\gamma^{\mu}\not{\epsilon}_{11}\not{k})\\
&\times\left(e^{i(\chi_1+\chi_2)}G_{N+n_1+n_2} - e^{i(\chi_1-\chi_2)}G_{N+n_1-n_2} + e^{-i(\chi_1-\chi_2)}G_{N-n_1+n_2} - e^{-i(\chi_1+\chi_2)}G_{N-n_1-n_2}\right)\\
&-\frac{\beta_{\rm i}\beta_{\rm f}(\mathcal{Z}e)^2A_{10}A_{20}}{16i(k\cdot p_{\rm i})(k\cdot p_{\rm f})}\sin\delta_1\cos\delta_2(\not{\epsilon}_{12}\not{k}\gamma^{\mu}\not{\epsilon}_{21}\not{k} + \not{\epsilon}_{21}\not{k}\gamma^{\mu}\not{\epsilon}_{12}\not{k})\\
&\times\left(e^{i(\chi_1+\chi_2)}G_{N+n_1+n_2} + e^{i(\chi_1-\chi_2)}G_{N+n_1-n_2} - e^{-i(\chi_1-\chi_2)}G_{N-n_1+n_2} - e^{-i(\chi_1+\chi_2)}G_{N-n_1-n_2}\right)\\
&+\frac{\beta_{\rm i}\beta_{\rm f}(\mathcal{Z}e)^2A_{10}A_{20}}{16(k\cdot p_{\rm i})(k\cdot p_{\rm f})}\sin\delta_1\sin\delta_2(\not{\epsilon}_{12}\not{k}\gamma^{\mu}\not{\epsilon}_{22}\not{k} + \not{\epsilon}_{22}\not{k}\gamma^{\mu}\not{\epsilon}_{12}\not{k})\\
&\times\left(e^{i(\chi_1+\chi_2)}G_{N+n_1+n_2} - e^{i(\chi_1-\chi_2)}G_{N+n_1-n_2} - e^{-i(\chi_1-\chi_2)}G_{N-n_1+n_2} + e^{-i(\chi_1+\chi_2)}G_{N-n_1-n_2}\right)\Bigg]u^{(\beta_{\rm i})}_{p_{\rm i},\lambda_{\rm i}}. \qquad (28)
\end{aligned}$$

From now on, we take over from our earlier works [21,25] the derivation of probability rates of e^-e^+ pair creation in laser-nucleus collisions, with an exact account for a nuclear recoil. For the convenience of the reader, we present in the following section the final formulas expressing the probability rates of the process under consideration.

C. Probability rates of pair production

As has been derived in Refs. [21,25], the total probability rates of electron-positron pair creation during the laser-nucleus impact process W is

$$\begin{aligned}
W \equiv \sum_N W_N = \sum_N \int d^3q_{\rm f}d^3p_{\rm e^-}d^3p_{\rm e^+}\sum_{\{\lambda\}}\frac{\mathcal{Z}^2\alpha^2m_{\rm e}^2M_{\rm N}^2c^9}{2\pi^3}\\
\times\frac{|t_N|^2}{E_{\boldsymbol{q}_{\rm i}}E_{\boldsymbol{q}_{\rm f}}E_{\boldsymbol{p}_{\rm e^-}}E_{\boldsymbol{p}_{\rm e^+}}}\delta^{(4)}(\bar{q}_{\rm i}-\bar{q}_{\rm f}-\bar{p}_{\rm e^-}-\bar{p}_{\rm e^+}+Nk).
\end{aligned} \qquad (29)$$

Similar to the monochromatic case [21,25], N is interpreted as a net number of photons absorbed from the laser field, whereas W_N in Eq. (29) defines the N-photon partial probability rate of pair creation. $\alpha = e^2/(4\pi\varepsilon_0 c)$ is the fine structure constant and $M_{\rm N}$ is the nucleus mass. Moreover, we keep $p_{\rm e^-}$ and $p_{\rm e^+}$ as the electron and positron four-momenta, respectively, $q_{\rm i}$ and $q_{\rm f}$ as the initial and the final nucleus four-momenta, all of them measured outside of the laser focus. On the contrary, $\bar{p}_{\rm e^-},\bar{p}_{\rm e^+},\bar{q}_{\rm i}$, and $\bar{q}_{\rm f}$ relate to the particles dressed by the laser field; these momenta are defined by Eq. (7). Hence, the delta function that is present in Eq. (29) determines the dressed four-momenta conservation condition. In Eq. (29), the symbol $\sum_{\{\lambda\}}$ stands for averaging with respect to the initial-spin and summation over the final-spin degrees of freedom of all particles,

$$\sum_{\{\lambda\}} = \frac{1}{2}\sum_{\lambda_{\rm i}=\pm}\sum_{\lambda_{\rm f}=\pm}\sum_{\lambda_{\rm e^-}=\pm}\sum_{\lambda_{\rm e^+}=\pm}. \qquad (30)$$

We have also introduced there the matrix element t_N,

$$\begin{aligned}
t_N = \sum_L \mathcal{C}^{\mu}_{N-L}(p_{\rm e^-}\lambda_{\rm e^-},p_{\rm e^+}\lambda_{\rm e^+})\tilde{\mathcal{D}}_{\mu\nu}(\bar{q}_{\rm i}-\bar{q}_{\rm f}+Lk)\\
\times\mathcal{F}^{\nu}_{L}(q_{\rm f}\lambda_{\rm f},q_{\rm i}\lambda_{\rm i}),
\end{aligned} \qquad (31)$$

which is the sum over all N-photon processes in which L laser photons are exchanged between the nucleus and the field. Defining the matrix t_N, we have used the following definitions:

$$\mathcal{C}_N^{\mu}(p_{e^-}\lambda_{e^-}, p_{e^+}\lambda_{e^+}) = \mathcal{J}_N^{\mu}(p_{e^-},\lambda_{e^-},1; p_{e^+},\lambda_{e^+}, -1), \quad (32)$$

$$\mathcal{F}_N^{\mu}(q_f\lambda_f, q_i\lambda_i) = \mathcal{J}_N^{\mu}(q_f,\lambda_f,1; q_i,\lambda_i,1), \quad (33)$$

where $\mathcal{J}_N^{\mu}$ is given by Eq. (28), and

$$\tilde{\mathcal{D}}_{\mu\nu}(\bar{q}_i - \bar{q}_f + Lk) = -\frac{g_{\mu\nu}}{(\bar{q}_i - \bar{q}_f + Lk)^2}. \quad (34)$$

At this point, let us note that the photon propagator (34) has poles if only $(\bar{q}_i - \bar{q}_f + Lk)^2 = 0$, and that these poles are the reason the matrix t_N diverges; the effect is known as the Oleinik resonances [25,32–35]. It has been recognized, however, in Ref. [22] that these resonances can be turned into finite resonances if a laser pulse, instead of a plane wave, is considered. For this reason, we modify the photon propagator such that instead of $1/Q^2$ we introduce $1/(Q^2 + i\epsilon)$ where ϵ relates to the laser pulse length τ such that $\epsilon = 2k^0/(c\tau)$. The same regularization of the photon propagator has been used in our most recent paper where the pair creation induced by a monochromatic laser field was considered [26].

III. RELATIVE PHASE EFFECTS

Our foregoing investigations focus on phase effects in the electron-positron pair-creation process by a two-mode laser field. In this section, we shall analyze angular distributions of product particles as they vary with the relative phase, $\chi \equiv \chi_2 - \chi_1$, of the two-color field.

To define angular distributions of produced electrons (positrons), let us go back to the definition of the partial probability rates of pair creation, W_N, given by Eq. (29). This equation can be simplified due to the presence of the corresponding delta function. As we have already shown in our previous work [21], this leads to

$$W_N = \sum_{\ell} \int dE_{\boldsymbol{q}_f} d\Omega_{\boldsymbol{q}_f} d\Omega_{\boldsymbol{p}_{e^-}} R_N^{(\ell)}(\boldsymbol{q}_f, \hat{\boldsymbol{p}}_{e^-}), \quad (35)$$

where $R_N^{(\ell)}(\boldsymbol{q}_f, \hat{\boldsymbol{p}}_{e^-})$ is the triply differential probability rate of pair production for the case when the value of energy transfer from the colliding nucleus as well as orientations of the nucleus and the created electron are fixed. We do not present here the explicit form of $R_N^{(\ell)}(\boldsymbol{q}_f, \hat{\boldsymbol{p}}_{e^-})$; however, for further details on derivations of $R_N^{(\ell)}(\boldsymbol{q}_f, \hat{\boldsymbol{p}}_{e^-})$ and its final form we encourage the reader to see Ref. [21]. At this point, let us only mention that the triply differential probability rate of pair creation is defined in terms of the matrix element t_N (31) where the summation over the number of photons L exchanged by the nucleus with the e^-e^+ pair occurs. As we recognized in our previous works on pair creation by a monochromatic laser field [21,25], in many cases one can disregard the dressing of the nucleus by the laser field. This is related to the fact that the correction to the rest-mass energy squared of the nucleus, due to the presence of the laser field, equals $(Z\mu m_e c^2)^2/2$, which is much smaller than the rest-mass energy squared of the nucleus itself. The same argument holds for a pair creation by a bichromatic laser field, which is considered in this paper. For this reason, we assume that there is a zero-photon exchange between the nucleus and the pair, $L = 0$. Thus, all the results presented here are for this case.

Before we proceed with presenting numerical results, let us remind the reader that, if the target particle is countermoving toward the laser beam at a large Lorentz factor γ, then in its rest frame both the laser frequency and the laser-field strength are increased by roughly a factor of 2γ [7–9]. In other words, for currently available ultra-intense laser pulses, the electric field experienced by the target particle during its collision with the laser beam approaches, in fact, the critical Schwinger value [36,37]. This makes it promising to observe experimentally the electron-positron pairs through the nonlinear Bethe-Heitler scenario. To make the process more effective, in the present and the subsequent sections, we consider the head-on configuration of a laser beam with a relativistic target. More precisely, we consider the situation when the laser field propagates along the z axis, such that the wave vector is $\boldsymbol{k} = -(\omega/c)\boldsymbol{e}_z$, and each component of the two-color field is linearly polarized with the polarization vector along the x axis. For a colliding nucleus we take a proton. From now on, all quantities are specified in the reference frame where the proton is initially at rest, meaning that $\boldsymbol{q}_i = \boldsymbol{0}$. Moreover, in this section we assume that the colliding proton is reflected in the direction of the laser field propagation, with $\boldsymbol{q}_f = -2m_e c\boldsymbol{e}_z$ (in the chosen reference frame).

At this point let us make a brief comment on recoil effects in laser-induced pair creation. We have investigated this problem in great detail in our recent papers dealing with pair creation by a monochromatic laser field [21,25,26]. In particular, in Ref. [21] we have demonstrated that a zero-momentum recoil is forbidden by the energy and momentum conservation laws. In addition, we have noted that the most pronounced signal of produced pairs is observed for the momentum transfer from the colliding particle roughly between $m_e c$ and $2m_e c$, which seems does not depend very much on the laser field parameters. Since the same stays true for the bichromatic case that is under investigation now, we present here numerical illustrations for a specific choice of the proton final momentum, as specified above. In fact, we have performed calculations for other choices of the proton momentum transfer which still lead to considerable signal of produced pairs. We have observed that, for smaller values of $\boldsymbol{q}_f$ and for typical parameters of the laser field considered in this paper, the pairs are produced in a very small cone along the propagation direction of the laser field. For the present choice of $\boldsymbol{q}_f$ we find, however, that the pairs can be produced in any direction with respect to $\boldsymbol{k}$, which makes this case particularly interesting for numerical illustrations. Here, the number of photons which are absorbed from the laser field, N, is fixed in order to analyze the dependence of $R_N(\boldsymbol{q}_f, \hat{\boldsymbol{p}}_{e^-}) = \sum_\ell R_N^{(\ell)}(\boldsymbol{q}_f, \hat{\boldsymbol{p}}_{e^-})$ on the electron detection angles, θ_{e^-} and φ_{e^-}.

Figures 1 and 2 show the angular maps of the triply differential probability rates of pair production by 5 laser photons ($N = 5$), $R_5(\boldsymbol{q}_f, \hat{\boldsymbol{p}}_{e^-})$, and by 183 laser photons ($N = 183$), $R_{183}(\boldsymbol{q}_f, \hat{\boldsymbol{p}}_{e^-})$, respectively. The results are for the case when, in the chosen reference frame, the Doppler up-shifted frequency of the basic-color field is $\omega = m_e c^2$, and where $n_1 = 1, n_2 = 2$, whereas the strengths of each field component are equal; $\mu_1 = \mu_2 = 1$ in Fig. 1 and $\mu_1 = \mu_2 = 10$ in Fig. 2.

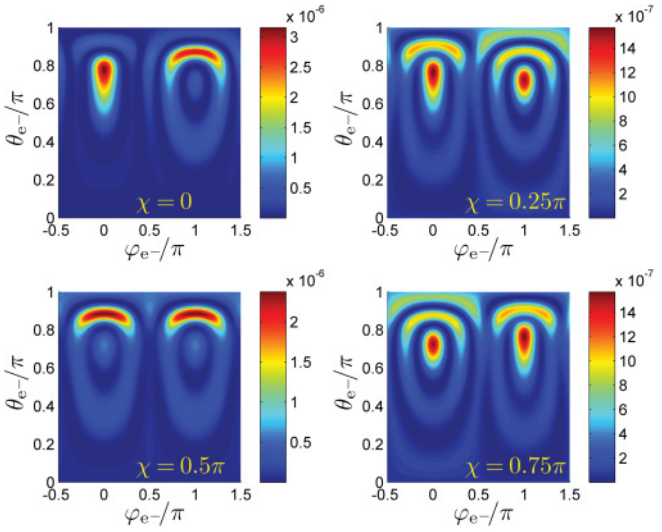

FIG. 1. (Color online) Angular maps of $R_5(\boldsymbol{q}_f, \hat{\boldsymbol{p}}_{e^-})$ for the case when $\omega = m_e c^2$ (in the chosen reference frame), $n_1 = 1$, $n_2 = 2$, and $\mu_1 = \mu_2 = 1$. The momentum transfer from the colliding proton is $\boldsymbol{q}_f = (0,0,-2m_e c)$. Each panel corresponds to a different relative phase of both color fields. Here, the angles θ_{e^-} and φ_{e^-} are the electron spherical angles measured in the coordinate frame such the z axis is in the opposite direction to the laser field propagation direction, whereas the x axis is along the polarization direction of both color fields.

The results are for chosen relative phases χ, as specified in each panel. In both figures, one can see that angular distributions of the created particles do depend on the relative phase of both color fields, which is similar to strong-field ionization in the nonrelativistic regime [2,38–40]. However, contrary to strong-field ionization in the nonrelativistic regime, in the case of pair creation, electrons are predominantly created at polar angles θ_{e^-} close to π, which is in the direction of the laser field propagation. The same has been observed for relativistic ionization [41,42] and has been

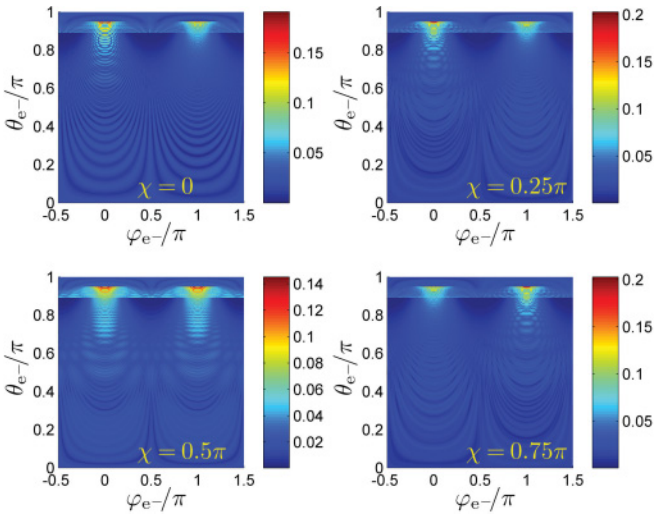

FIG. 2. (Color online) Same as Fig. 1 but for the 183-photon pair-creation process, $R_{183}(\boldsymbol{q}_f, \hat{\boldsymbol{p}}_{e^-})$, and for an even stronger laser field such that $\mu_1 = \mu_2 = 10$. For visual purposes, the rates $R_{183}(\boldsymbol{q}_f, \hat{\boldsymbol{p}}_{e^-})$ have been raised to power 1/5.

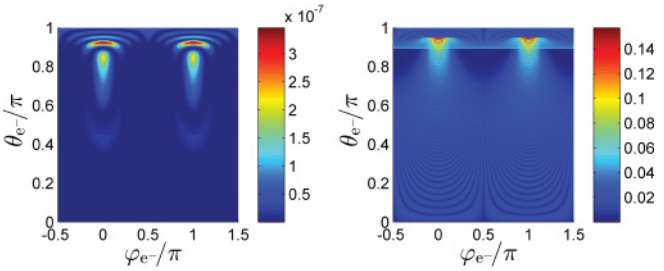

FIG. 3. (Color online) Angular maps of $R_5(\boldsymbol{q}_f, \hat{\boldsymbol{p}}_{e^-})$ (left panel) for the case when $\omega = m_e c^2$, $\mu_1 = \sqrt{2}$, and $\mu_2 = 0$. The right column shows $R_{183}(\boldsymbol{q}_f, \hat{\boldsymbol{p}}_{e^-})$ for the same parameters except that $\mu_1 = 10\sqrt{2}$. In each case, the momentum transfer from the colliding proton is $\boldsymbol{q}_f = (0,0,-2m_e c)$. For visual purposes, the rates $R_{183}(\boldsymbol{q}_f, \hat{\boldsymbol{p}}_{e^-})$ have been raised to power 1/5.

realized to be a general feature of nonperturbative multiphoton phenomena that involves ultrastrong laser fields. As was stated in Refs. [41,42], while in the relativistic regime the motion of electrons in the direction of the laser field propagation is driven by the magnetic component of the Lorentz force, in the nonrelativistic regime this effect is marginal. In particular, for nonrelativistic strong-field ionization by a linearly polarized laser field, the photoelectrons are detected in the direction of the polarization vector. One may argue that the nonrelativistic ionization rates are more sensitive to instantaneous value of the electric field component than the rates of pair creation or the rates of relativistic ionization. The former is confirmed by the present calculations of the total probability rates of pair creation, which appear to be independent of the relative phase of both color fields. The total probability rates of nonrelativistic strong-field ionization, on the other hand, do depend on the relative phase of the bichromatic laser field (see, for instance, [2,39,40]). We are not aware however of any calculations for ionization by a bichromatic laser field in the relativistic domain, which makes further comparison impossible.

Comparing Figs. 1 and 2, one can note that created particles are more focused around the laser field propagation direction in Fig. 2 than in Fig. 1, which is for a bigger momentum transfer from the laser photons. This is forced by the four-momentum conservation condition which, for a bigger momentum transfer from the laser beam, can be satisfied only if the created particles basically follow the propagation direction of laser photons. In Fig. 2, one can also observe two very distinct thresholds, which appear at θ_{e^-} close to π, and which do not depend on the relative phase χ. With similar thresholds we have dealt in the monochromatic case considered in Ref. [21]. These were recognized to mark borders between different sectors of pair creation, as defined by the four-momentum conservation condition (for more details, see [21]). Since this conservation condition has only one solution for the parameters chosen in Fig. 1, there is no similar threshold observed there. In fact, results for pair creation by a monochromatic laser field are also presented here. In Fig. 3, we show angular maps for 5-photon pair creation by a monochromatic laser field (left panel) for the case when $\omega = m_e c^2$, $\mu_1 = \sqrt{2}$, and $\mu_2 = 0$. In the right panel, we show similar results for the 183-photon process such that $\mu_1 = 10\sqrt{2}$. The results are for the rescaled

parameter μ_1 such that the threshold energy of pair creation is the same as in Figs. 1 or 2 (see discussion in Sec. IV). As one can see, also in the monochromatic case there are no similar borders for 5-photon pair production, whereas they appear for the 183-photon process. Let us also mention that similar sectors do not appear in nonrelativistic strong-field ionization, since in this case the energy conservation condition has only one solution. Moreover, the presented angular distributions for both mono- and bichromatic cases show sidelobes, the number of which increases with increasing the number of absorbed laser photons. As we have already argued in Ref. [21], these sidelobes are observed due to interference of different paths along which the process can be realized (for an illustration, see Fig. 2 of Ref. [21]). In addition, in the case of a bichromatic laser field, different numbers of photons from each color-field can be absorbed with significant probabilities. Since for the chosen parameters characterizing the bichromatic laser field there is fewer significant paths necessary for the same N-photon process to occur, as compared to the monochromatic case, fewer sidelobes in angular distributions are also observed. This is very clear when comparing Fig. 1 and the left panel of Fig. 3, which are for the 5-photon process. For higher-photon processes the same stays true, although an additional structure can also appear (see right panel of Fig. 3 as compared to Fig. 2 for the 183-photon process).

As we have already mentioned, even though the angular distribution of pair creation does depend on the relative phase of both color fields, the total probability rates of pair creation practically do not depend on this phase. It is more interesting, therefore, to analyze the carrier-envelope phase effects in the pair-creation process, which shall be done in the following sections.

IV. CHOICE OF SHAPE FUNCTION

In order to analyze the carrier-envelope phase effects in the nonlinear Bethe-Heitler process we need to account for a finite laser pulse or for a train of laser pulses. Let us concentrate on the latter case. Thus, we describe a train of linearly polarized laser pulses for which the four-vector potential can be written as

$$A^\mu(k\cdot x) = A_0\varepsilon^\mu f\,(k\cdot x,\{\chi\})\,, \tag{36}$$

with f being the shape function such that it can depend on various phase-related parameters $\{\chi\}$. Even though the theory developed in this paper is not strictly applicable to treat pulse trains, we will demonstrate in the next section that it can still be used in a particular case. The case that we have in mind is the pulse train described by the following shape function:

$$f_{\rm train}(k\cdot x,\chi) = \sin^4(k\cdot x)\sin(k\cdot x+\chi), \tag{37}$$

where χ is the so-called carrier-envelope phase.

A. Shape function $f(k\cdot x,\chi)$

Let us analyze the bichromatic laser field that is linearly polarized, meaning that $\delta_1 = \delta_2 = 0$ and $\varepsilon_{i1} \equiv \varepsilon$ (for $i = 1,2$) in Eq. (2). In other words, the actual form of the four-vector potential describing a two-color field is given by Eq. (36). More specifically, we take the following shape function describing the two-color laser field:

$$f(k\cdot x,\chi) = \tfrac{1}{16}[6\sin(k\cdot x+\chi) + 4\sin(k\cdot x-\chi) - 4\sin(3k\cdot x+\chi) - \sin(3k\cdot x-\chi)], \tag{38}$$

which can be also written as

$$f(k\cdot x,\{\chi\}) = f_1\cos(n_1 k\cdot x+\chi_1) + f_2\cos(n_2 k\cdot x+\chi_2), \tag{39}$$

where $n_1 = 1$ and $n_2 = 3$, and where

$$f_1 = \tfrac{1}{8}\sqrt{1+24\cos^2\chi}, \quad \tan\chi_1 = -5\cot\chi, \tag{40}$$

$$f_2 = \tfrac{1}{16}\sqrt{9+16\cos^2\chi}, \quad \tan\chi_2 = -\tfrac{5}{3}\cot\chi. \tag{41}$$

One can easily see that, in the present case, the laser field has only the first and the third harmonics. At this point, it is important to realize that the chosen shape function gives a good approximation of the laser pulse train (37). In Fig. 4, we present a comparison of the shape function $f(k\cdot x,\chi)$ [Eq. (38)] with the exact shape of the laser pulse train $f_{\rm train}(k\cdot x,\chi)$ [Eq. (37)] for two chosen phases $\chi = 0$ and $\chi = \pi/2$. One can see a very good agreement between both shape functions for $\chi = 0$ which deteriorates however for $\chi = \pi/2$. In fact, one can check that both functions (37) and (38) differ by a term,

$$f_{\rm train}(k\cdot x,\chi) - f(k\cdot x,\chi) = \tfrac{1}{16}\sin(5k\cdot x+\chi), \tag{42}$$

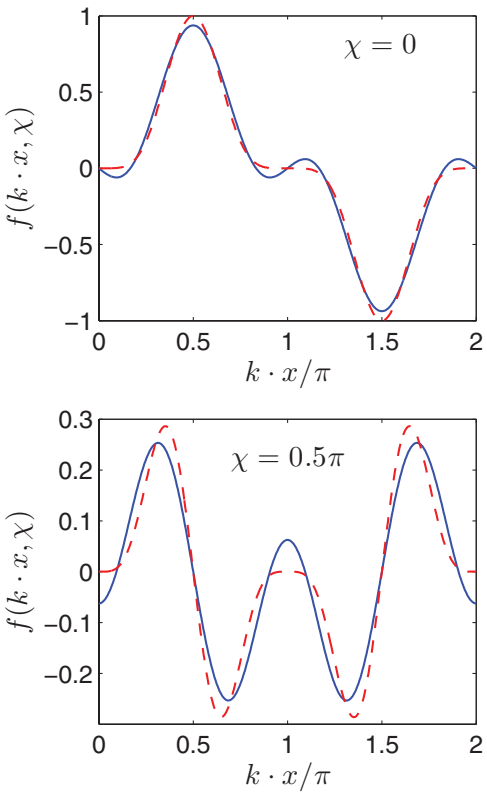

FIG. 4. (Color online) Comparison of two shape functions $f_{\rm train}(k\cdot x,\chi)$ given by Eq. (37) (red dashed line) and $f(k\cdot x,\chi)$ described by Eq. (38) (blue solid line) for chosen values of the carrier-envelope phase χ [$\chi = 0$ (upper panel) and $\chi = \pi/2$ (lower panel)].

that contains the fifth harmonic. This suggests that, in order to treat the above-mentioned pulse train (37) exactly, one would need to develop the respective formalism for a three-color field. This is, however, beyond the scope of the present paper.

For convenience, from now on we shall refer to Eq. (38) rather than to Eq. (39) when discussing the shape function f. Thus let us note that the function under consideration (38) can be also represented as

$$f(k\cdot x,\chi)=\sum_{N=-\infty}^{\infty} f_N(\chi)e^{-iNk\cdot x}, \tag{43}$$

where the only nonzero harmonics are

$$f_1(\chi)=f^*_{-1}(\chi)=\frac{1}{32i}(-6e^{-i\chi}-4e^{i\chi}), \tag{44}$$

$$f_3(\chi)=f^*_{-3}(\chi)=\frac{1}{32i}(4e^{-i\chi}+e^{i\chi}). \tag{45}$$

As one can understand, the temporal shape of the electric field corresponding to this shape function depends critically on the carrier-envelope phase χ. In general, this is the case for any laser field characterized by a carrier-envelope phase. Consequently, a process like ionization (see, for instance, Ref. [43]) or a nonlinear Bethe-Heitler process depends strongly on χ. The latter will be illustrated in Sec. V.

Except for $f(k\cdot x,\chi)$, let us also define the normalized shape functions $f_{\mathrm{U}}(k\cdot x,\chi)$ and $f_{\mathrm{I}}(k\cdot x,\chi)$ such that the ponderomotive energy of the free particle's oscillations in the two-color laser field or the mean intensity carried by the two-color laser field, respectively, do not depend on the carrier-envelope phase χ. This is particularly important when comparing the probability rates of a given process that is induced by different laser pulses, or by different laser-pulse trains. Let us note that, in general, for multichromatic laser fields with specified relative phases discussed in Sec. III, both the ponderomotive energy and the mean laser-field intensity do not depend on those phases. The situation is different however for laser fields which are characterized by the carrier-envelope phase.

B. Shape function $f_{\mathrm{U}}(k\cdot x,\chi)$

It is important to realize that the pair-creation threshold energy depends on the ponderomotive energy of an electron (positron) U that moves freely in a laser field. More precisely, the threshold energy for the electron-positron pair-creation process is $2\bar{m}_{\mathrm{e}}c^2$, where the dressed mass of electron is such that $(\bar{m}_{\mathrm{e}}c)^2=(m_{\mathrm{e}}c)^2+2m_{\mathrm{e}}U$. Let us recall that the ponderomotive energy U is the cycle-averaged energy of the charged particle's quiver oscillations in a laser field. For a particle of charge $\mathcal{Z}e$ and a four-momentum p, one can define it as a zero-component of the following four-vector:

$$U_\mu=\left\langle-\frac{(\mathcal{Z}e)^2A^2(k\cdot x)}{2p\cdot k}\right\rangle ck_\mu, \tag{46}$$

where $\langle\cdots\rangle$ stands for averaging with respect to the field oscillations. For the electron ($\mathcal{Z}=1$), the ponderomotive energy in its rest frame of reference is

$$U=U_0=\left\langle-\frac{e^2A^2(k\cdot x)}{2m_{\mathrm{e}}}\right\rangle, \tag{47}$$

which in our case gives

$$U=\frac{(eA_0)^2}{2m_{\mathrm{e}}}\langle f^2(k\cdot x,\chi)\rangle=\frac{1}{2}m_{\mathrm{e}}c^2\mu^2\langle f^2(\chi)\rangle. \tag{48}$$

Here and in all subsequent sections, μ is defined as $\mu=\frac{|eA_0|}{m_{\mathrm{e}}c}$. In addition, we understand that

$$\langle f^2(\chi)\rangle=\frac{1}{2\pi}\int_0^{2\pi}d\phi f^2(\phi,\chi). \tag{49}$$

As we have mentioned before, for a bichromatic laser field characterized by a carrier-envelope phase χ, the ponderomotive energy depends on χ. This can be illustrated for the case discussed in Sec. IV A, for which the ponderomotive energy equals

$$U=\tfrac{1}{2^{10}}m_{\mathrm{e}}c^2\mu^2(13+112\cos^2\chi). \tag{50}$$

One can expect therefore that the rate of pair production would be smaller in this case for $\chi=0$ than for $\chi=\pi/2$, because for $\chi=\pi/2$ the ponderomotive energy (50) (and so the threshold energy) is minimal. This may suggest that, in order to compare the rates of pair creation for different envelope phases χ, one should in fact compare the results obtained for such shape functions,

$$f_{\mathrm{U}}(k\cdot x,\chi)=N_{\mathrm{U}}(\chi)f(k\cdot x,\chi), \tag{51}$$

that would lead to the same ponderomotive energy. This can be accomplished, for instance, if the condition

$$\left\langle f^2_{\mathrm{U}}\right\rangle=\frac{1}{2\pi}\int_0^{2\pi}d\phi f^2_{\mathrm{U}}(\phi,\chi)=\frac{1}{2} \tag{52}$$

is imposed; here, the normalization constant is chosen to correspond to the monochromatic case. In closing this section, let us note that in order to satisfy Eq. (52) for the case considered in Sec. IV A, one has to use the following normalization $N_{\mathrm{U}}(\chi)$:

$$\frac{1}{N_{\mathrm{U}}(\chi)}=\sqrt{\frac{1}{2^8}(13+112\cos^2\chi)}. \tag{53}$$

Thus, introducing a similar Fourier decomposition of the function $f_{\mathrm{U}}(k\cdot x,\chi)$ as given by Eq. (43),

$$f_{\mathrm{U}}(k\cdot x,\chi)=\sum_{N=-\infty}^{\infty} f_{\mathrm{U},N}(\chi)e^{-iNk\cdot x}, \tag{54}$$

we obtain that

$$f_{\mathrm{U},N}=N_{\mathrm{U}}(\chi)f_N(\chi), \tag{55}$$

where the only nonvanishing harmonics are those with $N=\pm1,\pm3$.

C. Shape function $f_{\mathrm{I}}(k\cdot x,\chi)$

Another choice of the shape function that is of physical significance when analyzing the phase effects in laser-induced processes would be to normalize it such that the mean intensity carried out by the laser field is phase independent. This also means that the mean energy of the laser field does not depend on the carrier-envelope phase, which we believe is the situation mostly met in experiments.

Let us remind the reader that the mean intensity of the laser field I is defined as the averaged over the period of oscillations T the energy flux of the electromagnetic field, represented by the Poynting vector [44]. Hence,

$$I = c\left(\frac{2\pi}{T}\right)^2 A_0^2 \varepsilon_0 \langle [f']^2 \rangle = \frac{m_e^2 c^3 \varepsilon_0 \mu^2}{e^2}\left(\frac{2\pi}{T}\right)^2 \langle [f']^2 \rangle, \tag{56}$$

where ε_0 is the vacuum permittivity and f' stands for the derivative of the shape function $f(k\cdot x,\chi)$ with respect to its first argument. One can check that for a monochromatic laser field,

$$I = \frac{m_e^2 c^3 \varepsilon_0 \mu^2 \omega^2}{2e^2}. \tag{57}$$

Having established this, we define the normalized shape function $f_{\rm I}(k\cdot x,\chi)$,

$$f_{\rm I}(k\cdot x,\chi) = N_{\rm I}(\chi) f(k\cdot x,\chi), \tag{58}$$

such that its derivative fulfills

$$\langle [f_{\rm I}']^2 \rangle = \frac{1}{2\pi}\int_0^{2\pi} [f_{\rm I}'(\phi,\chi)]^2 d\phi = \frac{1}{2}. \tag{59}$$

As we can understand from Eq. (56), each shape function satisfying the above condition leads to the same average laser field intensity (57). We find out that in the case considered in this paper [i.e., when f is given by Eq. (38)], this is achieved if only

$$\frac{1}{N_{\rm I}(\chi)} = \sqrt{\frac{1}{2^8}(85 + 240\cos^2\chi)}. \tag{60}$$

Having this in mind, we can also introduce the Fourier expansion of the respective shape function, such that

$$f_{\rm I}(k\cdot x,\chi) = \sum_{N=-\infty}^{\infty} f_{{\rm I},N}(\chi) e^{-iNk\cdot x}, \tag{61}$$

with

$$f_{{\rm I},N} = N_{\rm I}(\chi) f_N(\chi), \tag{62}$$

and $N = \pm 1, \pm 3$.

The phase dependence of the normalization coefficient $N_{\rm I}(\chi)$ is shown in the last panel of Fig. 5. In the same panel, the phase dependence of the normalization constant $N_{\rm U}(\chi)$ is also illustrated. Both of these coefficients show a double-hump structure which shows pronounced peaks for $\chi = \pi/2$ and $\chi = 3\pi/2$. One can also observe that $N_{\rm I}(\chi)$ exhibits more smooth dependence on χ than $N_{\rm U}(\chi)$. In the remaining panels of Fig. 5, we show each shape function $f(k\cdot x,\chi)$, $f_{\rm I}(k\cdot x,\chi)$, and $f_{\rm U}(k\cdot x,\chi)$ for chosen phases: $\chi = 0, \pi/4$, and $\pi/2$. In each case, we observe three maxima whose relative heights change, however, depending on the value of χ. For each shape function, the most modified shapes are achieved for $\chi = \pi/2$.

In Fig. 6, we present modulus of the first and the third harmonic components for three different shape functions, namely, $f_N(\chi)$ (blue dash-dotted line), $f_{{\rm U},N}(\chi)$ (solid red line), and $f_{{\rm I},N}(\chi)$ (black dashed line), where N is either 1 or 3. Depending on normalization, we note a qualitative difference between $f_{{\rm U},N}(\chi)$ and $f_{{\rm I},N}(\chi)$, as compared to $f_N(\chi)$. The difference is not very obvious for the first harmonic, as each

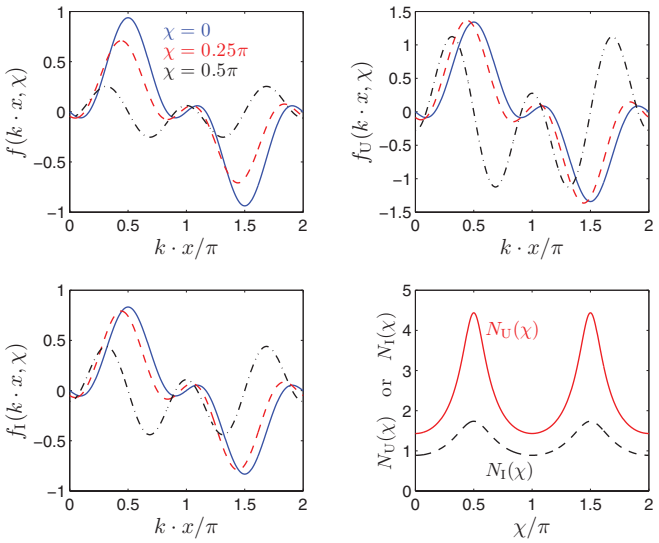

FIG. 5. (Color online) Shape functions $f(k\cdot x,\chi)$, $f_{\rm U}(k\cdot x,\chi)$, and $f_{\rm I}(k\cdot x,\chi)$ [defined by Eqs. (38), (51), and (58), respectively] for three chosen values of the carrier envelope phase χ [$\chi = 0$ (blue solid line), $\chi = 0.25\pi$ (red dashed line), and $\chi = 0.5\pi$ (black dash-dotted line)]. The last panel shows the dependence of the normalization factors $N_{\rm U}(\chi)$ and $N_{\rm I}(\chi)$ on the phase χ.

shape function exhibits a minimum at $\chi = \pi/2$ and $3\pi/2$. The situation changes for the third harmonic. In this case, $f_3(\chi)$ exhibits a minimum at the above-mentioned values, whereas $f_{{\rm U},3}(\chi)$ and $f_{{\rm I},3}(\chi)$ show maxima there. These maxima are particularly pronounced for $f_{{\rm U},3}(\chi)$. As we shall recognize later on, this difference dramatically modifies the total probability rates of pair creation, when comparing them for different shape functions.

V. CARRIER-ENVELOPE PHASE EFFECTS

Here we present the results for total probability rates of pair creation, which were obtained for each of the discussed shape functions defining the laser field. In doing so, we use the Monte Carlo method developed in Ref. [11]. In Fig. 7, we show the respective total rates of pair production that were calculated for different values of the envelope phase $\chi_i = i\pi/8$, where $i = 0,\ldots,16$. Each of the calculated values was obtained as the average of more than 10^9 sample points in each Monte Carlo run. The relative standard deviation for these data was estimated between 0.001 and 0.01. The results presented are still for $\omega = m_e c^2$ (in the reference frame where $\boldsymbol{q}_{\rm i} = \boldsymbol{0}$) and for different values of the parameter μ such that $\mu = 0.01$, 0.1, and 1 (from bottom to top). The data corresponding to different shape functions are marked as diamonds [for $f(k\cdot x,\chi)$], circles [for $f_{\rm U}(k\cdot x,\chi)$], and squares [for $f_{\rm I}(k\cdot x,\chi)$]. Even though for a given shape function, the dependence of total probability rates on the phase χ is very similar regardless μ, one should recognize that the rates grow in magnitude significantly with increasing the parameter μ. By comparing Fig. 6 and Fig. 7, we also observe that qualitative behavior of total probability rates of pair creation presented in Fig. 7 is dominated by the behavior of the third harmonic. Thus, the question arises whether the one-photon pair-creation process

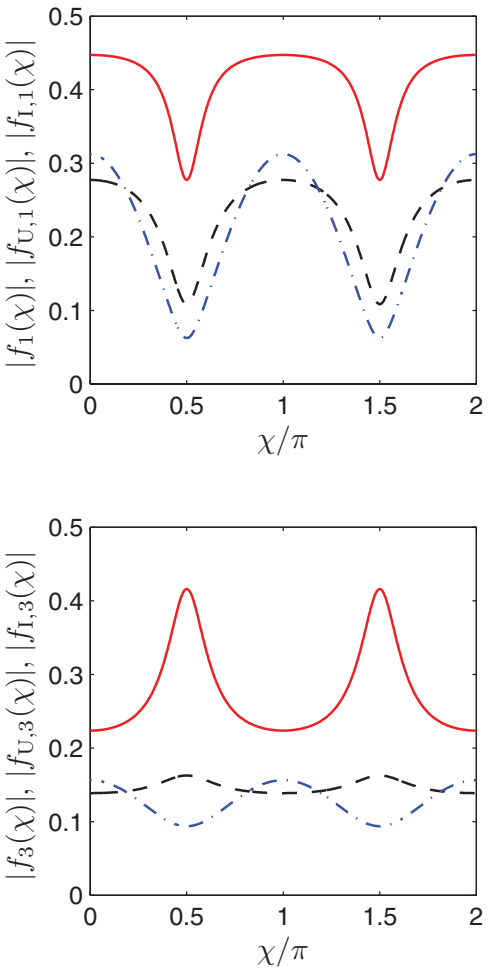

FIG. 6. (Color online) Modulus of the first and the third harmonic components for three shape functions considered in this paper; the solid red line corresponds to $f_{U,N}(\chi)$, the black dashed line is for $f_{I,N}(\chi)$, whereas the blue dash-dotted line is for $f_N(\chi)$.

by the 3ω laser field is dominant in this case. To answer this question, we analyze the ratio of the total probability rates of pair creation $R(\chi)$ and the intensity carried out by the third harmonic, $H^{[3]}(\chi)$,

$$R^{[3]}(\chi) = \frac{R(\chi)}{H^{[3]}(\chi)}. \tag{63}$$

Here, $H^{[3]}(\chi)$ is defined as $\mu^2|f_3(\chi)|^2$ for the unnormalized shape function, $\mu^2|f_{3,U}(\chi)|^2$ in the case of the shape function normalized with respect to the ponderomotive energy experienced by an electron in the two-color field, whereas $\mu^2|f_{3,I}(\chi)|^2$ is for the shape function normalized with respect to the intensity of the two-color field. Let us note that, if the one-photon process by the third harmonic was indeed dominant, the ratio defined by Eq. (63) should not depend on the phase χ, and should be the same for all normalizations considered. In Fig. 8, we show the respective ratio as a function of the phase χ for the laser field parameters $\omega = m_e c^2$ (in the chosen reference frame) and $\mu = 1$. In the upper panel, the results for the normalized shape functions are presented such that circles correspond to the choice of $f_U(k\cdot x,\chi)$

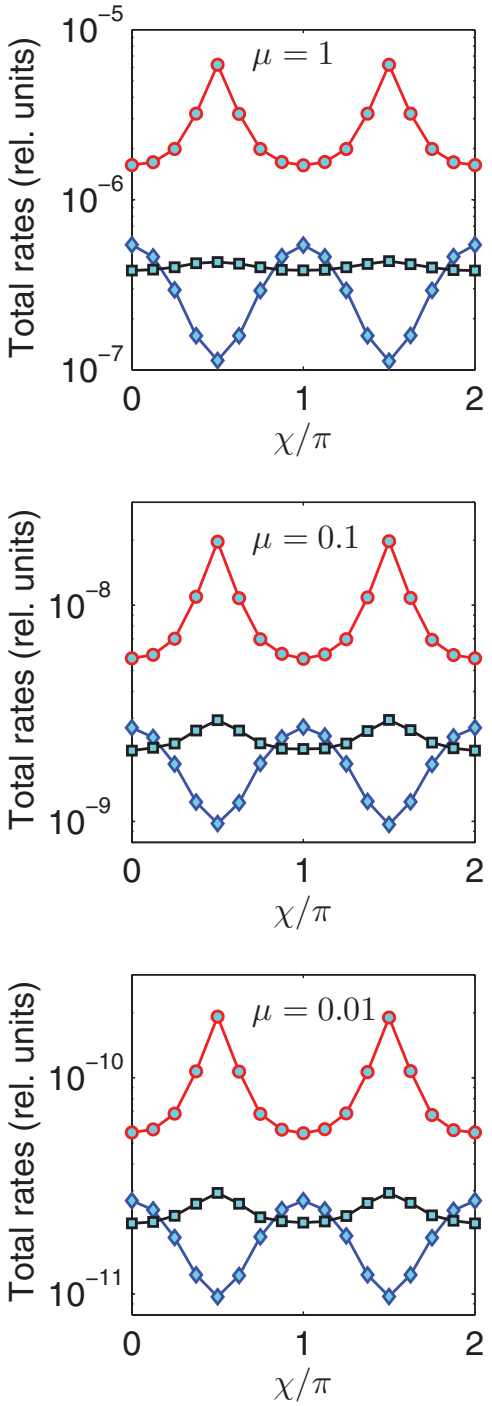

FIG. 7. (Color online) Total probability rate of pair creation as a function of the phase χ for the case when the laser-field frequency is $\omega = m_e c^2$ (in the chosen reference frame), whereas $\mu = 1$ (upper-most panel), $\mu = 0.1$ (middle panel), and $\mu = 0.01$ (lower-most panel). In each panel, the results obtained for different shape functions discussed in this paper [i.e., $f(k\cdot x,\chi)$ (diamonds), $f_U(k\cdot x,\chi)$ (circles), and $f_I(k\cdot x,\chi)$ (squares)] are presented.

whereas squares are for $f_I(k\cdot x,\chi)$. In the lower panel of Fig. 8, we show the results obtained for the unnormalized shape function $f(k\cdot x,\chi)$. Since none of the considered cases show a constant behavior as a function of χ, we conclude that interference of the one-photon and the three-photon processes

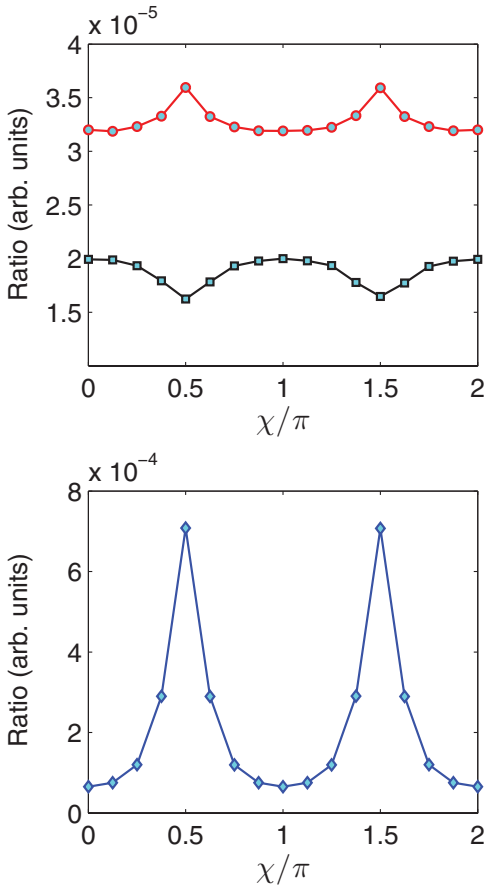

FIG. 8. (Color online) Dependence of the ratio defined by Eq. (63) on the carrier-envelope phase χ for $\omega = m_e c^2$ (in the chosen reference frame) and $\mu = 1$. In the upper panel, we present the results for the case when the shape function is either normalized with respect to the ponderomotive energy (circles) or with respect to the intensity of the laser field (squares). In the lower panel, the results for the unnormalized shape function are shown (diamonds).

plays here a crucial role. A qualitatively different situation is met for less-intense laser fields, particularly for the laser fields described by the parameters $\mu = 0.01$ and $\mu = 0.1$. Even though we do not present here the respective results, we have checked that in these cases the ratio defined by Eq. (63) exhibits a flat dependence on the carrier-envelope phase χ and is independent on the chosen normalization. This proves that, for weaker laser fields, the one-3ω-photon process is dominant, which is a perturbative result.

It follows from our analysis that, while in the case considered in this paper and for the laser field corresponding to $\mu = 0.01$, or 0.1 we deal with a perturbative pair creation, thus for $\mu = 1$ the process has a nonperturbative character. In the latter case, we conclude from Fig. 8 that the efficiency of pair production by the 3ω component of the laser field, which is defined by Eq. (63), does depend on the envelope phase χ in a nontrivial way. Also from Fig. 8, we see a qualitative difference between the results obtained for different shape functions of the laser field. In the case when the shape function is either not normalized or normalized with respect to the ponderomotive energy, we observe a maximum for the envelope phases $\chi = \pi/2$ and $3\pi/2$. On the opposite, if the shape function is normalized with respect to the intensity of the laser field, we see a dip for those values of χ. This proves that there is a strong interference between probability amplitudes which lead to the same final state of created particles.

In closing this section, let us comment on a flat phase-dependence of total probability rates of pair creation in the case when the shape function is normalized with respect to the laser field intensity (see Fig. 7). As we have mentioned before, such a χ-dependence of the total probability rates for the shape function $f_{\mathrm{I}}(k \cdot x, \chi)$ is governed by a similar flat behavior of $f_{\mathrm{I},3}(\chi)$ and thus is characteristic to our choice of the shape function. If we choose the same shape function $f(k \cdot x, \chi)$ to characterize the electric field, rather than the vector potential, the normalization to the laser field intensity in this case will correspond to the normalization introduced in Sec. IV B for $f_{\mathrm{U}}(k \cdot x, \chi)$. We have checked that, for this new choice of the shape function, a more significant carrier-envelope-phase dependence of total probability rates can be observed for the intensity-like normalization. In order to analyze this issue for other choices of the shape function, a more general approach developed for a multicolor laser field is necessary. This is beyond the scope of this paper but will be analyzed in the near future.

VI. CONCLUSIONS

We have studied electron-positron pair creation in the laser-nucleus-beam collisions, where a laser field has been modeled as a two-color field, and where nuclear recoil has been taken into account. We have analyzed the case where the frequencies of the two color-fields are commensurate. In particular, we have considered the superposition of the first and the third harmonic of the laser field, which is particularly interesting in the context of pair creation by a pulsed laser field.

Our main objective was to study phase effects in the laser-induced pair-creation process. We have observed a very pronounced dependence of angular distributions of the created pairs on the relative phase of a two-color field. On the contrary, the total probability rates of pair creation have turned out to be independent on the relative phase of a bichromatic laser field. For this reason, we have proceeded with analyzing the carrier-envelope phase effects in the case of a laser pulse train, which we have approximated by a bichromatic laser field. In this case, we have analyzed different forms of the four-vector potential describing the two-color laser field: the unnormalized one and normalized such that either the ponderomotive energy of the free particle oscillations in the two-mode laser field or the mean intensity carried by this field is independent of a carrier-envelope phase. For typical parameters of the laser field considered in this paper, which are in the nonperturbative regime, we have observed very pronounced interference effects in both angular distributions of created particles and in total probability rates of pair creation. The next step will be to analyze similar effects in the pair-creation process by a single laser pulse, which however requires to develop a new mathematical and numerical approach. This is under investigation now.

ACKNOWLEDGMENTS

This work is supported by the Polish National Science Center (Grant No. 2011/01/B/ST2/00381). K.K. gratefully acknowledges the hospitality of the Department of Physics and Astronomy, the University of Nebraska, Lincoln, Nebraska, USA, where part of this article was prepared.

[1] M. Shapiro and P. Brumer, Rep. Prog. Phys. **66**, 859 (2003).
[2] F. Ehlotzky, Phys. Rep. **345**, 175 (2001).
[3] F. Ehlotzky, K. Krajewska, and J. Z. Kamiński, Rep. Prog. Phys. **72**, 046401 (2009).
[4] V. P. Yakovlev, Zh. Eksp. Teor. Fiz. **49**, 318 (1965) [Sov. Phys. JETP **22**, 223 (1966)].
[5] M. H. Mittleman, Phys. Rev. A **35**, 4624 (1987).
[6] E. P. Liang, S. C. Wilks, and M. Tabak, Phys. Rev. Lett. **81**, 4887 (1998).
[7] C. Müller, A. B. Voitkiv, and N. Grün, Phys. Rev. A **67**, 063407 (2003).
[8] C. Müller, A. B. Voitkiv, and N. Grün, Phys. Rev. Lett. **91**, 223601 (2003).
[9] C. Müller, A. B. Voitkiv, and N. Grün, Phys. Rev. A **70**, 023412 (2004).
[10] P. Sieczka, K. Krajewska, J. Z. Kamiński, P. Panek, and F. Ehlotzky, Phys. Rev. A **73**, 053409 (2006).
[11] J. Z. Kamiński, K. Krajewska, and F. Ehlotzky, Phys. Rev. A **74**, 033402 (2006).
[12] K. Krajewska, J. Z. Kamiński, and F. Ehlotzky, Laser Phys. **16**, 272 (2006).
[13] A. I. Milstein, C. Müller, K. Z. Hatsagortsyan, U. D. Jentschura, and C. H. Keitel, Phys. Rev. A **73**, 062106 (2006).
[14] M. Yu. Kuchiev and D. J. Robinson, Phys. Rev. A **76**, 012107 (2007).
[15] K. Krajewska and J. Z. Kamiński, Laser Phys. **18**, 185 (2008).
[16] C. Deneke and C. Müller, Phys. Rev. A **78**, 033431 (2008).
[17] C. Müller, Phys. Lett. B **672**, 56 (2009).
[18] E. Lötstedt, U. D. Jentschura, and C. H. Keitel, New J. Phys. **11**, 013054 (2009).
[19] S. J. Müller and C. Müller, Phys. Rev. D **80**, 053014 (2009).
[20] A. Di Piazza, E. Lötstedt, A. I. Milstein, and C. H. Keitel, Phys. Rev. A **81**, 062122 (2010).
[21] K. Krajewska and J. Z. Kamiński, Phys. Rev. A **82**, 013420 (2010).
[22] H. Hu, C. Müller, and C. H. Keitel, Phys. Rev. Lett. **105**, 080401 (2010).
[23] A. Di Piazza, A. I. Milstein, and C. Müller, Phys. Rev. A **82**, 062110 (2010).
[24] T.-O. Müller and C. Müller, Phys. Lett. B **696**, 201 (2011).
[25] K. Krajewska, Laser Phys. **21**, 1275 (2011).
[26] K. Krajewska and J. Z. Kamiński, Phys. Rev. A **84**, 033416 (2011).
[27] V. I. Ritus, Tr. Fiz. Inst. Akad. SSSR **111**, 5 (1979).
[28] A. Yu and H. Takahashi, Phys. Rev. E **57**, 2276 (1998).
[29] N. B. Narozhny and M. S. Fofanov, Phys. Rev. E **60**, 3443 (1999).
[30] N. B. Narozhny and M. S. Fofanov, Zh. Eksp. Teor. Fiz. **117**, 476 (2000) [JETP **90**, 415 (2000)].
[31] D. M. Volkov, Z. Phys. **94**, 250 (1935).
[32] V. P. Oleinik, Zh. Eksp. Teor. Fiz. **52**, 1049 (1967) [Sov. Phys. JETP **25**, 697 (1967)].
[33] V. P. Oleinik and I. V. Belousov, *The Problems of Quantum Electrodynamics of the Vacuum, Dispersive Media and Strong Fields* (Kishinev, Shtiintsa, 1983).
[34] S. P. Roshchupkin, Laser Phys. **6**, 837 (1996).
[35] P. Panek, J. Z. Kamiński, and F. Ehlotzky, Phys. Rev. A **69**, 013404 (2004).
[36] F. Sauter, Z. Phys. **69**, 742 (1931).
[37] J. Schwinger, Phys. Rev. **82**, 664 (1951).
[38] R. M. Potvliege and P. H. G. Smith, J. Phys. B **25**, 2501 (1992).
[39] D. A. Telnov, J. Wang, and Shih-I. Chu, Phys. Rev. A **51**, 4797 (1995).
[40] K. J. Schafer and K. C. Kulander, Phys. Rev. A **45**, 8026 (1992).
[41] M. Klaiber, K. Z. Hatsagortsyan, and C. H. Keitel, Phys. Rev. A **75**, 063413 (2007).
[42] C. Müller, K. Z. Hatsagortsyan, M. Ruf, S. J. Müller, H. G. Hetzheim, M. C. Kohler, and C. H. Keitel, Laser Phys. **19**, 1743 (2009).
[43] D. B. Milošević, G. G. Paulus, D. Bauer, and W. Becker, J. Phys. B **39**, R203 (2006).
[44] D. J. Griffiths, *Introduction to Electrodynamics* (Prentice-Hall, Englewood Cliffs, 1999).